

Excellence in Chemistry Research

Announcing our new flagship journal

- Gold Open Access
- Publishing charges waived
- Preprints welcome
- Edited by active scientists



Meet the Editors of *ChemistryEurope*



Luisa De Cola
Università degli Studi
di Milano Statale, Italy



Ive Hermans
University of
Wisconsin-Madison, USA



Ken Tanaka
Tokyo Institute of
Technology, Japan



Ligand-Free Silver Nanoparticles for CO₂ Electrocatalytic Reduction to CO

Francesco Mattarozzi,^[a] Nienke Visser,^[a] Jan Willem de Rijk,^[a] Peter Ngene,^{*[a]} and Petra de Jongh^{*[a]}

Silver-based catalysts are attractive for electroreduction of CO₂ to CO. To understand the electrocatalyst properties, a good control over the nanoparticle size is necessary. Herein, we report a strategy to synthesize highly dispersed, ligand-free silver Ag nanoparticles supported on carbon. We demonstrate that the heat treatment atmosphere and carbon surface chemistry are crucial to control the Ag particle size in the 10–30 nm range. Even at low silver loadings (0.099 m²_{Ag} m⁻²), Ag

nanoparticles outperforms the bulk silver at low overpotentials, leading to a 23.5% CO Faradaic efficiency at –1.2 V vs RHE. The Ag weight-based activity of the catalysts scales with the inverse particle size, while the Ag surface-specific activity is independent of the particle size in this range. The supported silver nanoparticles can produce a H₂ to CO ratio of 2.9 to 1, interesting for further exploration of this type of catalysts for syngas synthesis.

Introduction

Anthropogenic carbon dioxide (CO₂) emissions are the major cause of climate change. In the latest Intergovernmental Panel on Climate Change report, it was estimated that greenhouse gas emissions have already caused global warming of approximately 1.0 °C above the pre-industrial levels.^[1] To mitigate climate change, renewable energy is given preference over fossil resources, but large-scale implementation is still a challenge. The main issues are the intermittent nature of wind and solar, and the lack of efficient large-scale electricity storage.^[2,3] ^[4] Electrocatalysis can convert CO₂ and H₂O to a range of value-added chemicals while using renewable electricity as the energy input.^[5–7] Furthermore, CO₂ reduction in an aqueous environment can be carried out under relatively mild conditions, and it is possible to control the reaction by adjusting external parameters such as the applied potential, the electrolyte composition, and CO₂ partial pressure.^[8] However, when the reaction is performed in water media, the competitive H₂ evolution lowers the selectivity.^[9] Therefore, the rational design of cathodic materials is essential.^[10]

In his pioneering work, Hori demonstrated that silver is one of the most promising transition metals for CO₂ reduction,

thanks to the high selectivity towards CO, a valuable chemical building block, compared to zinc and other transition metals.^[11–13] Many groups focus on the development of nanostructured silver catalysts supported on conductive substrates, to maximize the activity of the costly metal.^[14–16] Control over the particle size is essential to study the relationship between the structural properties of the catalyst and the electrochemical performance. In literature, colloidal synthesis of silver nanoparticles is often reported, as it can give good control over the nanoparticle size and morphology.^[17–22] However, the presence of ligands, which are difficult to remove, hampers studies of the intrinsic catalytic properties of silver nanoparticles. On the other hand the synthesis of ligand-free silver particles is challenging.^[23] To increase the stability of the metal catalyst, the silver nanoparticles are often supported on high surface area materials. Despite the high selectivity towards hydrogen formation, carbon offers many advantages as a support material for the silver nanoparticles for fundamental studies, such as good electrical conductivity, and the possibility to tune the silver particle size and the carbon support properties, which can influence the catalytic performance.^[24–26] Unfortunately, often a high metal weight loading and high mobility of silver species on carbon supports lead to sintering of the nanoparticles at moderate temperatures, leading to large particle size and broad particle distribution.^[27–28]


In this work, we employ a novel approach to control the particle size of ligand-free silver nanoparticles supported on carbon by Incipient Wetness Impregnation (IWI). We investigated the effect of different decomposition atmospheres and densities of carbon surface groups. We achieved reasonable control over the particle size, and we correlated specific electrochemical parameters (the CO Faradaic efficiency, CO partial current density and the H₂ to CO ratio) to morphological properties of the silver, such as particle size and surface coverage.


[a] F. Mattarozzi, N. Visser, J. W. de Rijk, Dr. P. Ngene, Prof. Dr. P. de Jongh
Materials Chemistry and Catalysis, Debye Institute for Nanomaterials
Science, Utrecht University, Universiteitsweg 99, Utrecht, The Netherlands
E-mail: p.ngene@uu.nl


p.e.dejongh@uu.nl

<https://www.uu.nl/medewerkers/PNgene>

<https://www.uu.nl/medewerkers/PEdeJongh>

 Supporting information for this article is available on the WWW under <https://doi.org/10.1002/ejic.202200365>

 Part of a joint Special Collection with ChemCatChem and EurJOC on the Netherlands Institute for Catalysis Research. Please click here for more articles in the collection.

 © 2022 The Authors. European Journal of Inorganic Chemistry published by Wiley-VCH GmbH. This is an open access article under the terms of the Creative Commons Attribution License, which permits use, distribution and reproduction in any medium, provided the original work is properly cited.

Results and Discussion

Control over the particle size

A first parameter that can be used to tune the silver particle size, is the composition of the atmosphere during the silver nitrate decomposition. We compared two samples: the first was treated in inert atmosphere (pure nitrogen, electron micrograph in Figure 1a) while the second was exposed to a reducing atmosphere (10% H₂ in nitrogen, electron micrograph in Figure 1b). All other variables, such as the silver loading on 100-P commercial carbon (10 wt%), the heat treatment temperature (250 °C) and gas hourly space velocity (6000 mL g_{cat}⁻¹ h⁻¹), were the same for both samples. Figure 1c and Figure 1d show the corresponding particle size distributions. In reducing atmosphere silver nanoparticles of 21 ± 15 nm were formed, while the treatment in inert atmosphere produced 34 ± 30 nm particles. This effect has been reported before^[23] and can be explained by the direct decomposition of AgNO₃ precursor to form Ag under H₂, while silver oxide intermediates are formed in inert atmosphere. Oxidized silver species are known to be highly mobile on the surface of the support, which can explain the larger particles and broad particle size distribution. Other reducing atmospheres with different gas composition (i.e. 30% H₂ in N₂) has been tested, but no beneficial effects were observed, rather larger particles and broad particle size distribution (Figure S3, SI). This is likely related to the fast kinetics of the decomposition reaction to form Ag nanoparticles on the carbon surface. Hence, 10% H₂/N₂ was used for all the samples.

After establishing the most promising gas composition to control the particle size, we further investigated the tunability of the particle size by using the same gas composition during the heat treatment (10% H₂ in N₂) but varying the surface

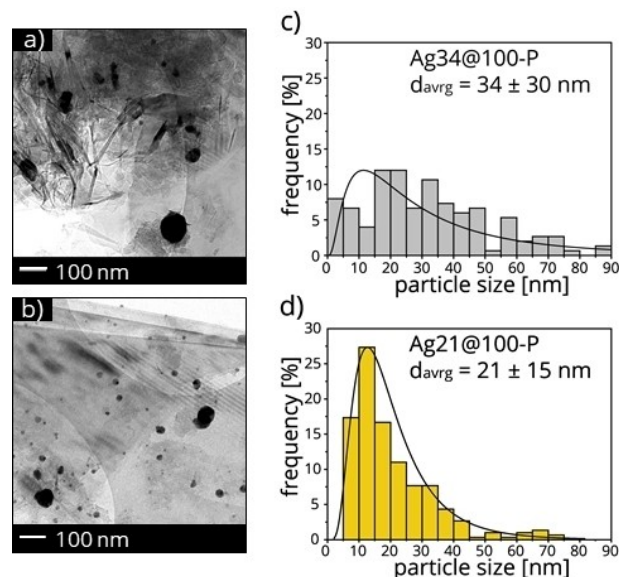


Figure 1. on the left, TEM images of (a) Ag34@100-P and (b) Ag21@100-P. On the right, particle size distribution of (c) Ag34@100-P and (d) Ag21@100-P.

properties of the carbon support. We compared the size of silver nanoparticles supported on four carbon materials, with different densities of acidic surface groups and surface areas (Table S1, SI). The commercial GNP500 support (in this work, 500-P) has a 5-fold larger surface area than HSAG100 (100-P) pristine carbon. Upon acidic functionalization, the surface areas of both carbon supports decreased by 40 m² g⁻¹, although the XRD patterns showed that the crystallinity of the carbon materials was not significantly affected (Figure S4, SI). Interestingly, after functionalization, both 100-O and 500-O showed a



Peter Ngene obtained his PhD in Chemistry in 2012 at Utrecht University in the Netherlands. He did a 3 years postdoc in the Chemical Engineering department, Delft University of Technology, before returning to Utrecht university as an assistant professor in the Materials Chemistry and Catalysis group, Debye Institute for Nanomaterials Science. Peter leads a research team that focuses on synthesis and advanced characterization of novel materials for efficient energy conversion and storage. This includes materials for next-generation batteries, fuel cells, reversible hydrogen storage, and electrochemical reduction of CO₂ to fuels/chemicals. Among other awards, he is the recipient of the Netherlands 2012/2013 KNCV-van Arkel best PhD thesis prize in Physical and Inorganic Chemistry, the Next Einstein Forum (NEF) fellowship from African Union as one of Africa's leading young scientists, and the NLNG-Nigerian Science Prize 2018 which is one of the highest science awards in Africa.



Petra de Jongh received her PhD in photoelectrochemistry in 1999, and worked 5 years as a senior scientist at Philips Research Laboratories in the Netherlands and Singapore. Since 2004 she works at Utrecht University where she holds the Chair Catalysts and Energy Materials in the MCC group. Her research focuses on supported nanoparticles and mesostructured materials, and gaining insight in the impact of particle size and distribution, confinement and pore structure on the functionality of these materials. An important application is the design of more efficient and durable catalysts, often in collaboration with industry, based for instance on studying the stability of supported metal nanoparticles under dynamic conditions. Another major research line is energy storage and conversion, including nanoconfined light metal hydrides for reversible hydrogen storage and fast ion conductors for all solid-state batteries. Recently her interests have expanded to include electrocatalytic and thermal CO₂ conversion.

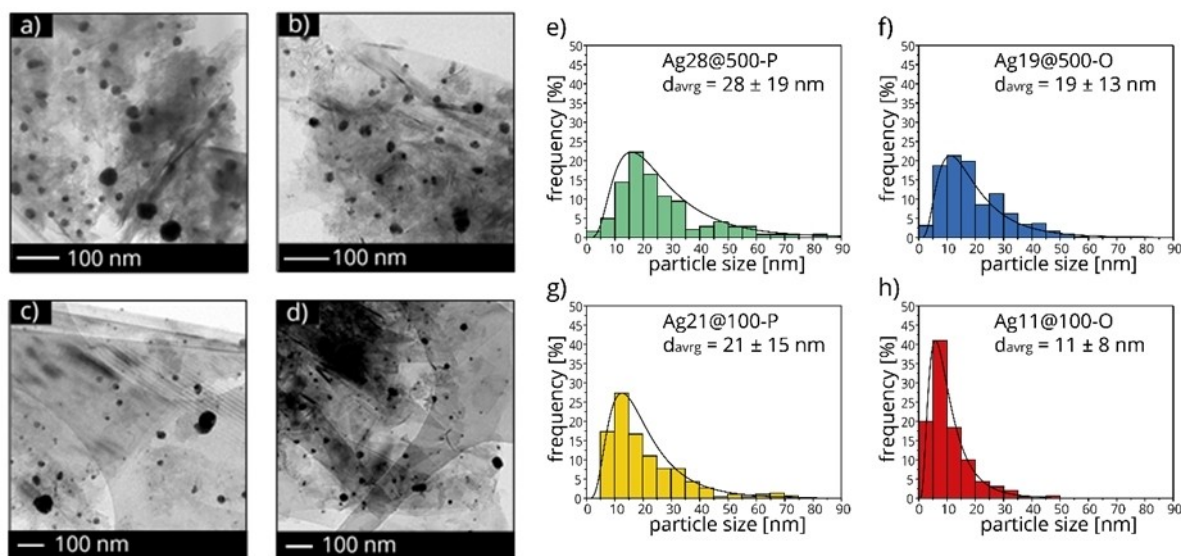


Figure 2. On the left, TEM images of Ag28@500-P (a), Ag19@500-O (b), Ag21@100-P (c) and Ag11@100-O (d). On the right, the corresponding particle size distributions of Ag28@500-P (e), Ag19@500-O (f), Ag21@100-P (g) and Ag11@100-O (h).

3-fold increase in the concentration of acid groups (Table S1, SI). With 1.75 groups per nm², 100-O showed a higher density of surface groups per unit of surface than 500-O with only 0.71 groups per nm² (Figure S5, SI).

Figure 2 (a–d) shows the TEM images of the Ag nanoparticles on the different supports and the corresponding particle size distribution (Figure 2 e–h). By comparing the images of the nanoparticles supported on the pristine (100-P and 500-P) and functionalized (100-O and 500-O) carbons, it is clear that a high number of surface groups led to small nanoparticles and narrower size distribution. Ag11@100-O presented an average particle size of 11 ± 8 nm, while Ag21@100-P showed a particle size of 21 ± 15 nm. Ag19@500-O showed a smaller particle size (19 nm) and less broad particle size distribution (13 nm) than the catalyst based on the pristine carbon (Ag28@500-P). In Figure 3, we related the particle size to the density of acid groups per unit of surface area. This correlation suggests that the surface groups act as nucleation and/or anchoring sites for the silver nanoparticles during the

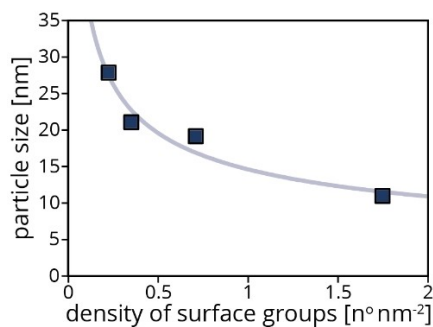


Figure 3. Ag particle size as a function of the density of functional groups on the surface of the carbon support. The blue line is added to guide the eye.

impregnation step. Since the pH of the precursor solution (6.0) was higher than the PZC of the support (Table S1, SI), it is likely that the silver cations interacted electrostatically with the deprotonated acid groups at the carbon support. Therefore, a higher number of surface groups per nm² might lead to a higher number of Ag nuclei, and, consequently, to a smaller Ag nanoparticle size.

Electrocatalytic activity

As more than 90% of our catalyst's exposed surface consisted of carbon, and carbon is known to be active to form H₂, we first studied the electrochemical activity of the supports. Figure 4a shows the total current densities of different carbon electrodes as a function of the applied potential, measured using chronoamperometry. The oxidized supports (i.e., 500-O and 100-O) produced a similar current density, with a maximum of −6.29 mA cm^{−2} at −1.4 V vs RHE, while the pristine support (100-P) generated a slightly smaller current density, with −5.70 mA cm^{−2} at the same potential. A similar trend is reported for the cyclic voltammetry measurements performed on the carbon support (Figure S6, SI). This observation can be explained by considering the surface properties of the carbons after the oxidation procedure. The high number of surface groups on 100-O and 500-O are expected to facilitate the electron transfer at the electrode-electrolyte interface.

Next, we consider the carbon supported Ag nanoparticles. Note that the effect of the oxidation state of silver nanoparticles is not discussed in this work. Although no silver oxide diffraction peaks were detected in the XRD analyses (Figure S7, SI) nor silver oxide reduction peaks during the cycle voltammetry scans of the supported catalysts (Figure S8, SI), we cannot exclude the presence of silver oxide at the surface, as the

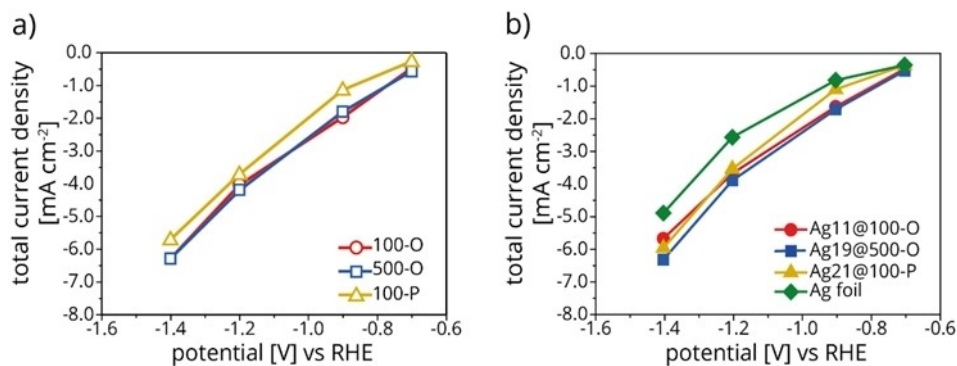


Figure 4. a) Total current density for the bare carbon supports 100-P, 100-O and 500-O as a function of the applied potential. b) Total current density for the supported silver catalysts Ag21@100-P, Ag11@100-O, Ag19@500-O and pure silver foil, as a function of the applied potential. In this figure, the current density is normalized to the geometric surface area of the electrode.

catalysts were exposed to the atmosphere. Nevertheless, the oxidation layer will affect all the catalysts in similar way, hence the obtained results do not strictly depend on it. Figure 4b shows the total current densities for the supported silver nanoparticles, measured using chronoamperometry at different applied potentials (Figure S9, SI). No significant differences were observed between the electrodes. Furthermore, by overlaying Figure 4a and Figure 4b, it is evident that the deposition of silver nanoparticles did not significantly change the electrochemical current compared to the bare supports. This result is perhaps not unexpected, given the low silver surface coverage, equal to 5% (Ag11@100-O) of the total carbon area. Therefore, we conclude that the current of the carbon-supported silver catalysts is dominated by the high surface area carbon support. However, by comparing our catalysts with the benchmark, we found that all the silver on carbon electrodes drew larger currents than the pure Ag foil. The smaller current density produced by the bulk flat electrode is likely due to its low electrochemical surface area (3.8 cm²). To unravel the effect of the silver nanoparticles on CO₂ reduction, we consider two crucial parameters: the CO Faradaic efficiency and the CO partial current density.

Effect of the silver coverage on the CO Faradaic efficiency

CO is the only product of CO₂ electroreduction expected for Ag catalysts, as no formate nor other liquid products was detected in the electrolyte, while H₂ evolution over carbon is the competitive reaction.^[29,30] Figure 5 shows the Faradaic efficiency (FE) towards CO, which is the fraction of electrons transferred contributing to the formation of CO, as a function of the silver surface fractional coverage, calculated as the m² of silver divided by the total catalyst surface, assuming hemispherical particles and using the average number particle size determined by TEM. The missing faradaic efficiency, up to 100%, is attributed to hydrogen. We chose the silver surface coverage as a key parameter to analyze the FE, since both silver and carbon contributed to the CO₂ electroreduction processes. The bare carbon 100-O (0.00 Ag fraction) produced mostly H₂ and only a

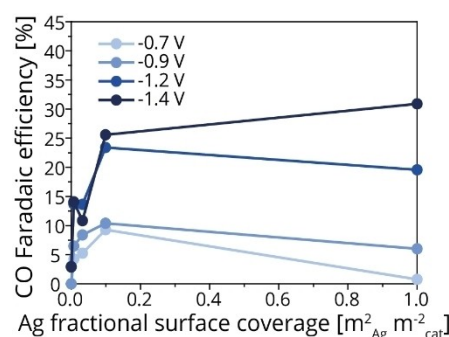


Figure 5. CO Faradaic efficiency comparison as a function of the Ag fractional coverage at the surface of the catalyst. Pure carbon = 0 m²_{Ag} m⁻²; Ag19@500-O = 0.007 m²_{Ag} m⁻²; Ag21@100-P = 0.032 m²_{Ag} m⁻²; Ag11@100-O = 0.099 m²_{Ag} m⁻²; bulk Ag electrode = 1 m²_{Ag} m⁻². The blue lines are added to guide the eye.

small amount of CO. On the contrary, Ag11@100-O (0.099 Ag fraction) gave a 25.6% CO FE at -1.4 V vs RHE. Although the HER dominates the FE, due to the high carbon surface area exposed to the electrolyte, a remarkably low concentration of silver nanoparticles and a low Ag surface fraction can significantly steer the selectivity of the electron transfer at the electrode surface towards CO₂ reduction. The evaluation of the selectivity at a given Ag fraction showed an increase of the CO FE with more negative potential. At constant potential, the CO FE increases as the Ag fraction increases. For instance, Ag11@100-O showed a 10.4% CO FE at very low overpotentials (-0.9 V vs RHE), while Ag21@100-P (0.032 Ag fraction) and Ag19@500-O (0.007 Ag fraction) produced only 8.4% and 6.5% CO FE at the same potential. The bulk silver electrode (1.00 Ag fraction, on the right side of Figure 5) showed a low CO FE at low overpotentials, with 6.0% CO FE at -0.9 V, even lower than Ag21@500-O. For higher overpotentials, the Faradaic efficiency to CO at the pure Ag foil electrode was similar to that of the supported Ag nanoparticles (5% surface coverage on carbon).^[31,32] Although catalytic data for intermediate silver surface fraction are missing, this analysis confirms the selective electron transfer via supported silver nanoparticles. A logical

approach to increase the CO FE would be to increase the silver weight loading. Unfortunately, by increasing the weight loading, we observed an uncontrolled particle growth, leading to a large particle size and broad particle size distribution (Figure S10, SI), hence the effects of the particle size cannot be reliably investigated.

Effect of the particle size on the CO partial current density

Figure 6 shows the CO partial current density as a function of the applied potential for both the carbon materials (Figure 6a) and the carbon supported silver nanoparticles (Figure 6b). As expected, the bare supports presented very low CO partial current densities, confirming that carbon support is highly selective towards the formation of H₂. Nevertheless, it seems that acidic surface groups slightly promote the CO₂ reduction, since 500-O produced a 1.6-fold and 10-fold higher CO partial current than 100-O and 100-P, respectively.

Figure 6b shows the CO current densities, normalized to the geometric surface area of the electrode of supported silver nanoparticles and the pure silver foil. The absolute values of the CO current density increased for all catalysts with the overpotentials. This increase became close to linear at large negative potentials, suggesting resistance-limited behavior,

probably due to diffusion limitations in the electrolyte solution. Additionally, we observed that Ag11@100-O, the catalysts with the smallest particle size, outperformed the other catalysts, generating a 1.6- and 2.2-times higher CO current density than Ag19@500-O and Ag21@100-P at -1.4 V vs RHE, respectively. Notably, Ag11@100-O gives a larger cathodic CO current density compared to the pure silver foil at low overpotentials. This might be explained by low-coordinated active sites at the surface of the silver nanoparticles readily stabilizing the CO intermediates, leading to an 0.4 mA cm⁻² larger cathodic current than the silver foil, at -1.2 V vs RHE.

In conclusion, the trend in CO current density demonstrates that the addition of silver nanoparticles to the carbon support, even at low weight loadings (10⁻⁴ g_{Ag} cm⁻²), increased remarkably the selectivity towards CO, while the high surface area carbon defines the total current density of the catalysts.

To understand the influence of Ag particle size, we analyzed the CO partial current density as a function of the average particle size (Figure 7). Figure 7a shows the absolute value of CO partial current density, normalized by the silver weight, measured at different potentials. It is clear that over the whole potential range, the CO partial current density is inversely proportional to the particle size. Furthermore, the particle size effect was enhanced at larger overpotentials. Ag11@100-O produced 6.7 mA mg_{Ag}⁻¹, while Ag19@500-O and Ag21@100-P

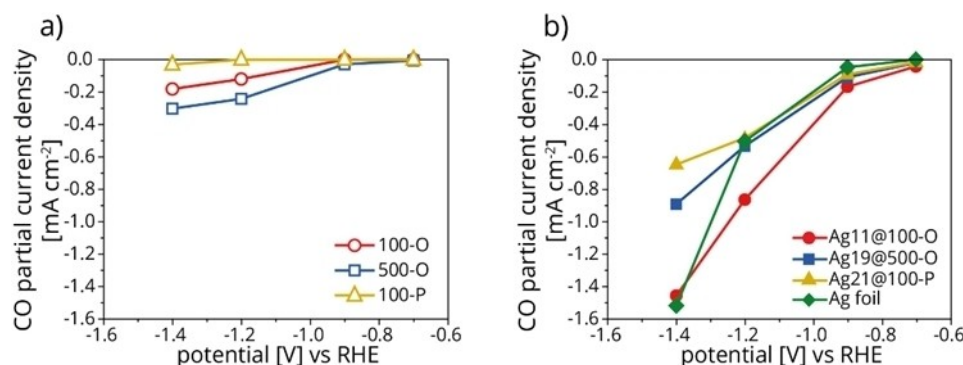


Figure 6. a) CO partial current density comparison for the bare carbon supports (empty markers) as a function of the applied potential. b) CO partial current density comparison for Ag supported catalysts (full markers), as a function of the applied potential. In this figure, the current density was normalized to the geometric surface area of the electrode.

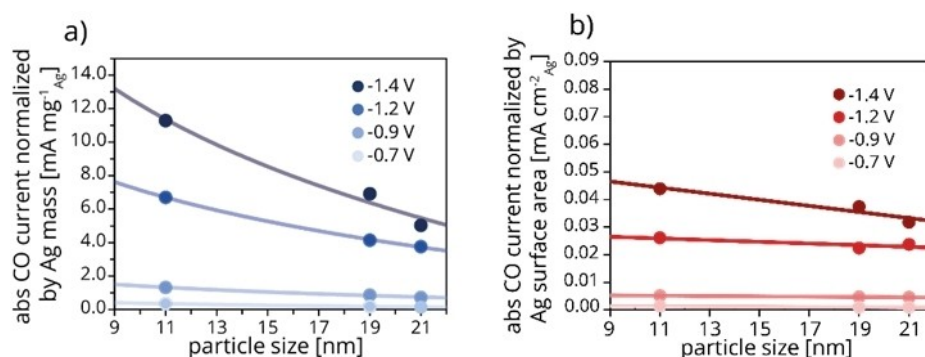


Figure 7. a) CO partial current density normalized by Ag weight on the electrode, as a function of the particle size. b) CO partial current density normalized by Ag surface area, as a function of the particle size. The interpolation lines are used to help understanding the figure.

generated only 4.1 mA $\text{mg}_{\text{Ag}}^{-1}$ and 3.7 mA $\text{mg}_{\text{Ag}}^{-1}$, respectively. This implies that either the smaller particles were intrinsically more active, or that it was simply an effect of specific surface area. Figure 7b shows the CO current density normalized to the silver surface area, calculated considering the particle size distribution obtained by TEM images (SI). This analysis reveals that the specific current density does not greatly depend on the particle size, and a weak trend is only observed at high overpotentials. Hence, there is no intrinsic difference between Ag11@100-O and other catalysts. The difference in CO FE when only the geometric surface areas are considered, is mainly due to the higher dispersion of the Ag on the carbon. Therefore, the remarkable catalytic performance (i.e. CO current density, CO FE) of Ag11@100-O is due to a higher surface to volume ratio for the smaller Ag nanoparticles.

H₂ to CO ratio

Since the electrochemical production of syngas, a mixture of hydrogen and carbon monoxide, might represent an opportunity to use 'green' hydrogen and CO to produce sustainable fuels, we evaluated the H₂ to CO ratio for the different catalysts. Figure 8 shows the H₂ to CO ratio as a function of the total current density. Ag11@100-O produced the lowest H₂ to CO ratio, compared to Ag19@500-O and Ag21@100-P, at all currents. For all the catalysts, the H₂ to CO ratio decreased at larger current densities, considering, for instance, that Ag11@100-O generated a minimum H₂ to CO ratio of 2.9 at the largest current density (-5.9 mA cm^{-2}). This behavior is probably due to an effect of the local pH on the reaction selectivity. Large current densities, generated at more cathodic potentials, result in proton consumption at the electrode-electrolyte interface. This phenomenon increases the local pH and steers the selectivity towards CO₂ reduction products by suppressing the H₂ evolution.^[33] Ag11@100-O gave a 3 to 1 H₂ to CO ratio at -1.2 V vs RHE (Figure S11, SI), a ratio that is close to be suitable to produce linear-chain alkanes via Fischer-Tropsch reaction. On the contrary, Ag19@500-O and Ag21@100-P exhibited an H₂ to CO ratio of only 6 to 1 at the same potential. This finding demonstrates that by tuning the particle size and the support surface properties, we can control the H₂ to CO ratio even at

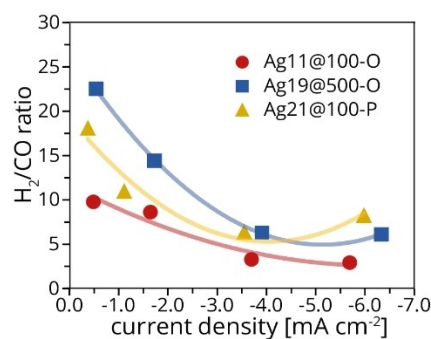


Figure 8. H₂ to CO ratio for the different catalysts, as a function of the total current density.

high current densities. Having said that, it has to be borne in mind that the current densities in these experiments are still much lower than required for industrial application.

Conclusion

We synthesized ligand-free silver nanoparticles supported on high surface area carbon materials via incipient wetness impregnation, achieving control over the particle size. We demonstrated the importance of the atmosphere during the heat treatment and the density of acidic surface groups to gain control over the particle size in the range of 11 nm to 21 nm. The total current density of the catalysts, during the CO₂ reduction in 0.1 M KHCO₃, was dominated by the high surface area of the carbon support producing H₂. Nevertheless, the presence of only 0.1 $\text{mg}_{\text{Ag}} \text{cm}^{-2}$ of silver on the carbon paper electrode effectively steered the selectivity to 25 % CO at -1.4 V vs RHE. Small nanoparticles of 11 nm produced higher CO currents than a bulk silver electrode. The mass activity of the catalysts decreased with increasing particle size, while the specific surface activity showed no dependence on the particle size. Hence, the remarkable catalytic performance of the small silver nanoparticles was achieved thanks to a good dispersion of the silver nanoparticles. The H₂ to CO ratio was as low as 2.9:1 at -5.9 mA cm^{-2} . This study contributes to the knowledge required for electrode design for CO₂ electrochemical reduction.

Experimental Section

XGnP500 graphene nanoplatelets were purchased from XG Science. HSAG100 high surface area graphite was provided by TIMREX. Silver nitrate (AgNO₃, 99%), HNO₃ (65% wt/wt), Nafion 117 solution, isopropanol (99.5%) and potassium bicarbonate (KHCO₃, >99%) were purchased from Sigma Aldrich. Regarding the electrochemical equipment, the proton selective Nafion N117 membrane was obtained from Ion Power, the glassy carbon was produced by HTW-Germany, the carbon paper substrate (TGP-H-060) by Toray, the platinum disc (99.5%) by Goodfellow and the Ag/AgCl 3 M reference electrode was purchased from Metrohm. The silver disc (99.95%, temper: as rolled), used as benchmark, was purchased from Goodfellow.

To study the influence of the support functional groups on the silver particle size, the commercial carbon powders GNP500 and HSAG100 were functionalized using nitric acid (65% wt/wt).^[34] Specifically, the carbon substrate (10 g) was dispersed in concentrated HNO₃ (50 $\text{mL}_{\text{HNO}_3} \text{ g}_{\text{carbon}}^{-1}$) in a 1 L round bottom flask equipped with a cooler. To avoid NO_x leaks during the procedure, two slightly basic (pH=8) water traps were connected to the head of the cooler. The reaction mixture was heated to 80 °C for 2 hours under vigorous stirring. Subsequently, the reaction mixture was quenched with cold water. The modified carbon was thoroughly washed with deionized water until the solution reached neutral pH, and then dried overnight at 90 °C in a round bottom flask. The effect of the functionalization procedure was evaluated by point of zero charge (PZC) analysis, potentiometric titration, N₂ physisorption and X-ray powder diffraction (XRD). The graphitic carbon supports were labelled with a number indicating the BET surface area of the pristine support and a letter, referring to the pristine (P) or oxidized (O).

The silver nanoparticles were deposited by incipient wetness impregnation.^[35] The carbon support was dried under vacuum at 170 °C for 2 hours, to remove moisture and air from the pores. Subsequently, the support was impregnated with an AgNO₃ aqueous solution under static vacuum at room temperature. The volume of the solution corresponded to 95% of the support pore volume and the AgNO₃ concentration varied between 2 M and 6 M, in order to achieve a silver weight loading of 10% for all the catalysts. After the impregnation step, the catalyst was dried under dynamic vacuum at room temperature for 10 hours, to remove the water and leave AgNO₃ nanocrystals on the surface of the carbon support. The dried catalyst was transferred to a fixed bed reactor (internal diameter 1 cm) and placed in the oven under a flow (6000 mL g⁻¹ h⁻¹) of 10% H₂ in N₂. The reactor was heated to 300 °C with a ramp of 5 °C min⁻¹, to decompose the AgNO₃ to Ag⁰. We refer to the Ag catalysts using a Agx@y-z nomination, where x is the mean particle size of the sample (i.e., Ag11, Ag19 and Ag21), y is the pristine support surface area and z is either P (pristine support) or O (oxidized support). For instance, Ag11@100-O refers to a catalyst with 11 nm Ag nanoparticles, supported on the oxidized (O) graphitic carbon support with 100 m² g⁻¹ surface area (100).

The working electrodes were prepared by spraying the supported silver catalysts (Ag21@100-P, Ag19@500-O and Ag11@100-O) on a carbon paper electrode (Toray TGP-H-060). The catalyst (11 mg) was dispersed in a water (4470 μL), isopropanol (1120 μL) and Nafion solution (44.4 μL) and sonicated for 45 minutes. This ink was then sprayed onto the carbon paper (4.9 cm²) and dried overnight at room temperature.^[36] A catalyst loading of 0.1 mg_{Ag} cm⁻² was intended for all the catalysts. A uniform distribution of the catalyst over the carbon paper support was demonstrated by SEM analysis (Figure S1, SI)

The BET surface area and the pore volume of the carbon support were probed via N₂-physisorption performed with a Micromeritics TriStar instrument at -196 °C. The carbon powder was dried at 170 °C under vacuum. Transmission electron microscopy (TEM) images of Ag19@500-O were acquired using Thermo Fischer Scientific Tecnai20 microscope, operated at 200 kV, while the TEM images of the other samples were acquired using TalosL120 C microscope, operated at 120 kV. The holey carbon 200 mesh copper grids were prepared by drop casting a mixture of ethanol and supported Ag catalysts, previously sonicated for 45 minutes. The Ag nanoparticle size was determined by measuring 300 particles at 5 different locations. The average particle size was calculated as

number average particle size: $average\ particle\ size = \frac{\sum_{i=1}^n d_n^3}{\sum_{i=1}^n d_n^2}$, where d_n is the diameter of particle n , and N is the total number of particles counted. X-ray diffraction (XRD) measurements were performed on a Bruker D2 Phaser, equipped with a Co K_α X-ray source with a wavelength of 1.79026 Å. The PZC of the support was measured by titration, using Milli-Q water as a solvent. This method involves the gradual addition of carbon material to 3 mL Milli-Q solution and continuous measurement of the pH. The pH of the solution saturates at high carbon concentrations, with the pH approaching the PZC of the support. The density of functional surface groups was evaluated by potentiometric titration using the TitraLab TIM880 Titration Manager apparatus. In particular, 20 mg of the sample was dispersed in 35 mL 0.1 M KCl solution and 0.01 M NaOH was used as the titrant.

A custom-built, three-electrode H-type electrochemical cell was used for the electrocatalytic experiments (Figure S2, SI). The cathodic compartment (volume = 11 mL) was separated from the anodic compartment (volume = 11 mL) by a Nafion membrane (Nafion N117). The CO₂ saturated catholyte was purged with 10 mL min⁻¹ CO₂ (Linde, purity 5.2), while the anolyte was stirred by

bubbling Ar. The working electrode was composed of a glassy carbon disc, in contact with the external electrical circuit and a carbon paper disc that was impregnated with the catalyst. The carbon paper surface area exposed to the electrolyte was 3.8 cm². We used a Ag/AgCl (3 M KCl) reference electrode and a 3.8 cm² Pt disc as counter electrode. A 0.5 M KHCO₃ solution (pH = 7) was used as electrolyte. All the electrochemical measurements were performed using an Autolab PGSTAT204 potentiostat, and the applied potential was converted to the reversible hydrogen electrode potential (RHE) using the equation: $E_{RHE} = E_{Ag/AgCl} + 0.209 + 0.059\ pH$.

The electrocatalytic performance was determined by chronoamperometry measurements at different potentials for 45 minutes. The gaseous products were analysed by connecting the cathodic compartment outlet to a Global Analysis Solutions Microcompact GC 4.0. The GC instrument was equipped with three channels. The first channel, a Rt-QBond (10 m*0.32 mm, Agilent) packed column, detects CH₄, C₂H₄ and C₂H₆, using a FID detector; the second channel, Molecular Sieve 5 A (10 m* 0.53 mm, Restek) packed column, that separates small gaseous molecules such as CO, and CH₄, is equipped with a methanizer, in order to increase the sensitivity for CO detection; the third channel, with a TCD detector, has a Carboxen 1010 (8 m*0.32 mm, Agilent) packed column which separates H₂ and CO₂. High purity nitrogen (N₂, 99.999%) was used as a carrier gas. The liquid products were analysed using a Varian HPLC with a refractive index detector (RID) and a Bio-Rad Aminex HPX-87H column at 60 °C. The Ag disc, used as benchmark, was mechanically polished using an alumina slurry before the electrochemical test.

The total current density analysis is crucial to compare the rate of the electron transfer across the electrode-solution interface, for different catalysts. We defined the total current density as the average current recorded at a specific potential, normalized by the geometrical surface area of the electrode (3.8 cm²). The Faradaic efficiency was calculated using the equation: $FE = \frac{(n \cdot F \cdot mol)}{i_{tot} \cdot t}$, where n were the moles of electrons per mole of product (mol_p, mol_e⁻), F represents the Faraday constant (C mol_e⁻), mol are the moles of products formed (mol_p), i is the total current (C s⁻¹) and t is the analysis time (s). Since the total Faradaic efficiency is very close to 100% for all catalysts, we preferred to normalize the value by 100, to fairly compare the samples. The partial current density defines the contribution of the individual reaction products to the total current density. This parameter was calculated as the product of the total current density and the FE. The silver surface area was calculated by using the particle size distribution (TEM images) and assuming that the particles were hemispheres (SI).

Acknowledgements

This work was funded by the Dutch Research Council (NWO), in collaboration with Advanced Research Center Chemical Building Blocks Consortium (ARC-CBBC) (project number: 2016.008) and Shell Global Solutions International B.V.. Kai Han is acknowledged for useful discussions regarding the electrochemical measurements.

Conflict of Interest

The authors declare no conflict of interest.

Data Availability Statement

The data that support the findings of this study are available from the corresponding author upon reasonable request.

Keywords: Carbon · CO₂ reduction · Electrochemistry · Particle size · Silver

- [1] V. Masson-Delmotte, P. Zhai, H.-O. Pörtner, D. Roberts, J. Skea, P. R. Shukla, A. Pirani, W. Moufouma-Okia, C. Péan, R. Pidcock, S. Connors, J. B. R. Matthews, Y. Chen, X. Zhou, M. I. Gomis, E. Lonnoy, T. Maycock, T. W. M. Tignor, World Meteorological Organization, Geneva, Tech. Rep. **2019**, .
- [2] V. Kumaravel, J. Bartlett, S. C. Pillai, *ACS Energy Lett.* **2020**, *2*, 486–519.
- [3] R. J. Detz, B. van der Zwaan, *Energy Policy* **2019**, *133*, 110938–110941.
- [4] J. C. Abanades, E. S. Rubin, M. Mazzotti, H. J. Herzog, *Energy Environ. Sci.* **2017**, *10*, 2491–2499.
- [5] K. Li, B. Peng, T. Peng, *ACS Catal.* **2016**, *6*, 7485–7527.
- [6] D. Chery, V. Lair, M. Cassir, *Front. Energy Res.* **2015**, *3*, 1–10.
- [7] L. Li, N. Zhao, W. Wei, Y. Sun, *Fuel* **2013**, *108*, 112–130.
- [8] P. De Luna, C. Hahn, D. Higgins, S. A. Jaffer, T. F. Jaramillo, E. H. Sargent, *Science* **2019**, *364*, 350–359.
- [9] A. Goyal, G. Marcandalli, V. A. Mints, M. T. M. Koper, *J. Am. Chem. Soc.* **2020**, *142*, 4154–4161.
- [10] D. L. T. Nguyen, Y. Kim, Y. J. Hwang, D. H. Won, *Carbon Energy* **2020**, *2*, 72–98.
- [11] Y. Hori, R. Takahashi, Y. Yoshinami, A. Murata, *J. Phys. Chem. B* **1997**, *101*, 7075–7081.
- [12] Y. Hori, K. Kikuchi, S. Suzuki, *Lab. Tech. Biochem. Mol. Biol.* **1990**, *20*, 5–51.
- [13] Y. Hori, S. Suzuki, *Bull. Chem. Soc. Jpn.* **1982**, *55*, 660–665.
- [14] N. J. Firet, T. Burdyny, N. T. Nesbitt, S. Chandrashekar, A. Longo, W. A. Smith, *Catal. Sci. Technol.* **2020**, *10*, 5870–5885.
- [15] J. T. Feaster, C. Shi, E. R. Cave, T. Hatsukade, D. N. Abram, K. P. Kuhl, C. Hahn, J. K. Nørskov, T. F. Jaramillo, *ACS Catal.* **2017**, *7*, 4822–4827.
- [16] M. Ma, B. J. Trzeźniewski, J. Xie, W. A. Smith, *Angew. Chem. Int. Ed.* **2016**, *55*, 9748–9752; *Angew. Chem.* **2016**, *128*, 9900–9904.
- [17] A. Louidice, O. Segura Lecina, R. Buonsanti, *ACS Materials Lett.* **2020**, *2*, 1182–1202.
- [18] S. E. Skrabalak, L. Au, X. Li, Y. Xia, *Nat. Protoc.* **2007**, *2*, 2182–2190.
- [19] Y. Sun, Y. Xia, *Science* **2002**, *298*, 2176–2179.
- [20] A. Tao, P. Sinsersuksakul, P. Yang, *Angew. Chem. Int. Ed.* **2006**, *45*, 4597–4601; *Angew. Chem.* **2006**, *118*, 4713–4717.
- [21] M. Wuthschick, B. Paul, R. Bienert, A. Sarfraz, U. Vainio, M. Sztucki, R. Kraehnert, P. Strasser, K. Rademann, F. Emmerling, J. Polte, *Chem. Mater.* **2013**, *25*, 4679–4689.
- [22] P. Y. Lim, R. S. Liu, P. L. She, C. F. Hung, H. C. Shih, *Chem. Phys. Lett.* **2006**, *420*, 304–308.
- [23] J. E. van den Reijen, S. Kanungo, T. A. J. Welling, M. Versluijs-Helder, T. A. Nijhuis, K. P. de Jong, P. E. de Jongh, *J. Catal.* **2017**, *356*, 65–74.
- [24] G. L. Chai, Z. X. Guo, *Chem. Sci.* **2016**, *7*, 1268–1275.
- [25] Z. Sun, T. Ma, H. Tao, Q. Fan, B. Han, *Chem* **2017**, *3*, 560–587.
- [26] J. Wu, R. M. Yadav, M. Liu, P. P. Sharma, C. S. Tiwary, L. Ma, X. Zou, X. Zhou, B. I. Yakobson, J. Lou, P. M. Ajayan, *ACS Nano* **2015**, *9*, 5364–5371.
- [27] R. Jiang, E. Moton, J. P. McClure, Z. Bowers, *Electrochim. Acta* **2014**, *127*, 146–152.
- [28] J. Guo, A. Hsu, D. Chu, R. Chen, *J. Phys. Chem. C* **2010**, *114*, 4324–4330.
- [29] J. Wu, S. Ma, J. Sun, J. I. Gold, C. Tiwary, B. Kim, L. Zhu, N. Chopra, I. N. Odeh, R. Vajtai, A. Z. Yu, R. Luo, J. Lou, G. Ding, P. J. A. Kenis, P. M. Ajayan, *Nat. Commun.* **2016**, *7*, 1–6.
- [30] N. Yang, S. R. Waldvogel, X. Jiang, *ACS Appl. Mater. Interfaces* **2016**, *8*, 28357–28371.
- [31] W. Yang, W. Ma, Z. Zhang, C. Zhao, *Faraday Discuss.* **2018**, *210*, 289–299.
- [32] S. A. Mahyoub, F. A. Qaraah, C. Chen, F. Zhang, S. Yan, Z. Cheng, *Sustain. Energy Fuels* **2019**, *4*, 50–67.
- [33] Y. Yoon, A. S. Hall, Y. Surendranath, *Angew. Chem. Int. Ed.* **2016**, *55*, 15282–15286; *Angew. Chem.* **2016**, *128*, 15508–15512.
- [34] R. Beerthuis, J. W. de Rijk, J. M. S. Deeley, G. J. Sunley, K. P. de Jong, P. E. de Jongh, *J. Catal.* **2020**, *388*, 30–37.
- [35] K. P. De Jong, *Synthesis of Solid Catalysts*, Wiley-VCH, **2009**, p. 408.
- [36] C. Kim, H. S. Jeon, T. Eom, M. S. Jee, H. Kim, C. M. Friend, B. K. Min, Y. J. Hwang, *J. Am. Chem. Soc.* **2015**, *137*, 13844–13850.

Manuscript received: June 7, 2022

Revised manuscript received: September 2, 2022

Accepted manuscript online: September 9, 2022